Tomographic Image Reconstruction

1 Introduction

- *Tomography* is a non-invasive imaging technique allowing for the visualization of the internal structures of an object without the superposition of over- and under-lying structures that usually plagues conventional projection images.

- For example, in a conventional chest radiograph, the heart, lungs, and ribs are all superimposed on the same film, whereas a computed tomography (CT) slice captures each organ in its actual three-dimensional position.

- Tomography has found widespread application in many scientific fields, including physics, chemistry, astronomy, geophysics, and, of course, medicine.

- While X-ray CT may be the most familiar application of tomography, tomography can be performed, even in medicine, using other imaging modalities, including ultrasound, magnetic resonance, nuclear-medicine, and microwave techniques.

- Each tomographic modality measures a different physical quantity:

    - *CT:* The number of x-ray photons transmitted through the patient along individual projection lines.
    - *Nuclear medicine:* The number of photons emitted from the patient along individual projection lines.
    - *Ultrasound diffraction tomography:* The amplitude and phase of scattered waves along a particular line connecting the source and detector.

- The task in all cases is to estimate from these measurements the distribution of a particular physical quantity in the object. The quantities that can be reconstructed are:

    - *CT:* The distribution of linear attenuation coefficient in the slice being imaged.
    - *Nuclear medicine:* The distribution of the radiotracer administered to the patient in the slice being imaged.
    - *Ultrasound diffraction tomography:* the distribution of refractive index in the slice being imaged.

- Remarkably, under certain conditions, the measurements made in each modality can be converted into samples of the *Radon transform* of the distribution that we wish to reconstruct. For example, in CT, dividing the measured photon counts by the incident photon counts and taking the negative logarithm yields samples of the Radon transform of the linear attenuation map.

- The Radon transform and its inverse provide the mathematical basis for reconstructing tomographic images from measured projection or scattering data.

2 The Radon Transform

- We will focus on explaining the Radon transform of an image function and discussing the inversion of the Radon transform in order to reconstruct the image.

- We will discuss only the 2D Radon transform, although some of the discussion could be readily generalized to the 3D Radon transform.

- The Radon transform (RT) of a distribution $f(x, y)$ is given by

$$p(\xi, \phi) = \int f(x, y)\delta(x \cos \phi + y \sin \phi - \xi) \, dx \, dy, \tag{1}$$

where δ is the Dirac delta function and the coordinates x, y, ξ, and ϕ are defined in the figure below.
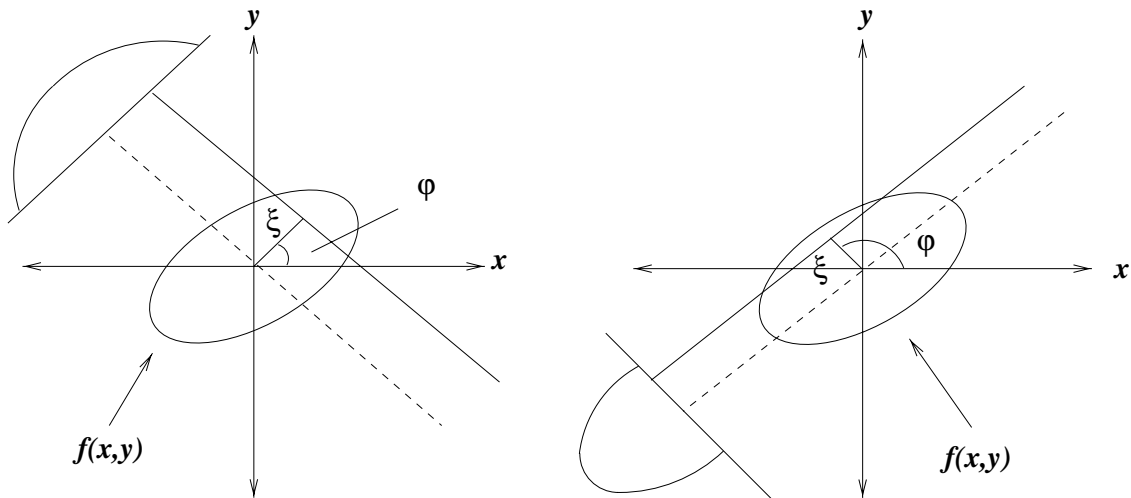
Figure 1. Coordinate system for the Radon transform.

- The function $p(\xi, \phi)$ is often referred to as a *sinogram* because the Radon transform of an off-center point source is a sinusoid.

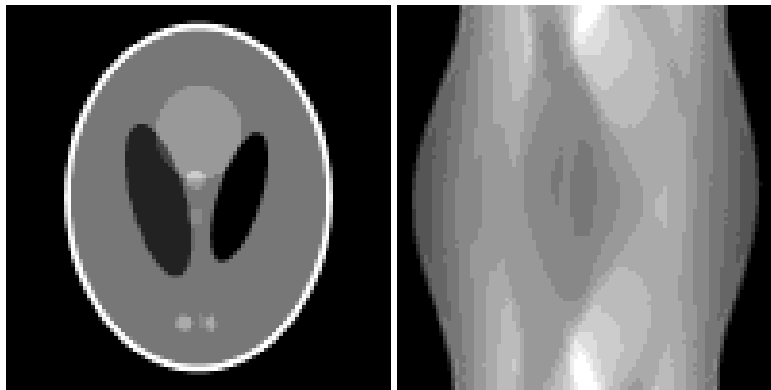- A typical slice image and its Radon transform are shown below:

Figure 2. Shepp-Logan phantom and its Radon transform.

- The task of tomographic reconstruction is to find $f(x, y)$ given knowledge of $p(\xi, \phi)$.

- The sinogram $p(\xi, \phi)$ has many nice mathematical properties, an important one of which is

$$p(\xi, \phi) = p(-\xi, \phi + \pi) \qquad (2)$$

3 Backprojection

- Mathematically, the backprojection operation is defined as:

$$f_{BP}(x, y) = \int_0^\pi p(x \cos \phi + y \sin \phi, \phi) d\phi \qquad (3)$$

- Geometrically, the backprojection operation simply propagates the measured sinogram back into the image space along the projection paths:
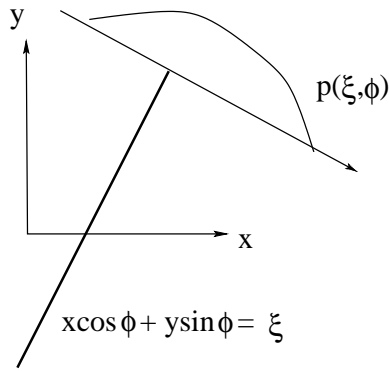
Figure 3. Geometrical interpretation of backprojection.

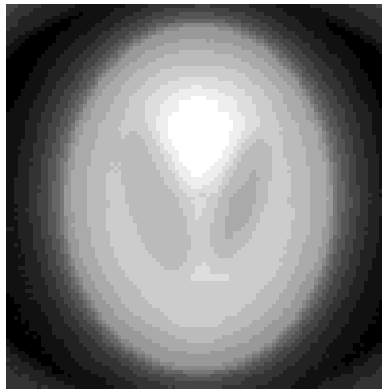- The backprojection image of the Shepp-Logan phantom is shown below:

Figure 4. The backprojection image of the Shepp-Logan phantom.

- Comparison of Figs. 2 and 4 shows that **the backprojection image is a blurred version of the original image.** Specifically,

  – For a point source at the origin $\delta(x, y)$, the intensity of the backprojection image rolls off slowly as $1/r$.
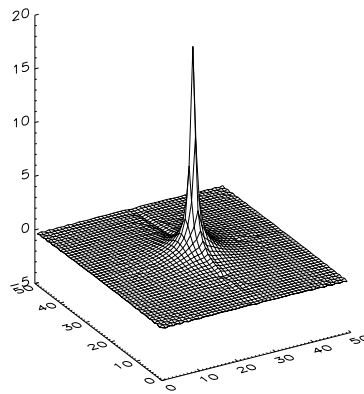

Figure 5. Surface plot of the backprojection image of a point source.

- Therefore, $f_{BP}(x, y) = \frac{1}{r} \star f(x, y)$, where $\star$ denotes the convolution operation.

4 Central Slice Theorem

- The solution to the inverse Radon transform is based on the central slice theorem (CST), which relates $F(\nu_x, \nu_y)$, the 2D Fourier transform (FT) of $f(x, y)$, and $P(\nu, \phi)$, the 1D FT of $p(\xi, \phi)$.

- Mathemtically, the CST is given by

$$P(\nu, \phi) = F(\nu \cos \phi, \nu \sin \phi). \tag{4}$$

- The CST theorem states that the the value of the 2D FT of $f(x, y)$ along a line at the inclination angle ϕ is given by the 1D FT of $p(\xi, \phi)$, the projection profile of the sinogram acquired at angle ϕ.
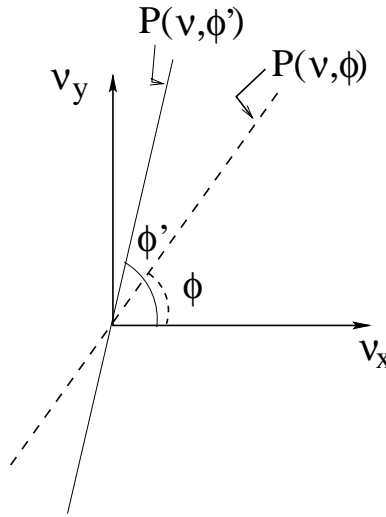

Figure 6. Central slice theorem.

- Hence, with enough projections, $P(\nu, \phi)$ can fill the $\nu_x - \nu_y$ space to generate $F(\nu_x, \nu_y)$.

- In the Fourier space, Eq. (2) becomes

$$P(\nu, \phi + \pi) = P(-\nu, \phi). \tag{5}$$

5 Reconstruction Approaches

There are many tomographic reconstruction techniques. Here, we consider only two of them.

- Direct Fourier reconstruction:

  - Once $F(\nu_x, \nu_y)$ is obtained from $p(\xi, \phi)$ using the CST, $f(x, y)$ can be obtained by applying inverse FT to $F(\nu_x, \nu_y)$.
  - <u>Issue of interpolation</u>: To utilize the fast Fourier transform (FFT) algorithm, values of $F(\nu_x, \nu_y)$ should be available at a rectangular grid. The values generated from the CST, however, are available at a polar grid. Fourier-space interpolation is therefore necessary.
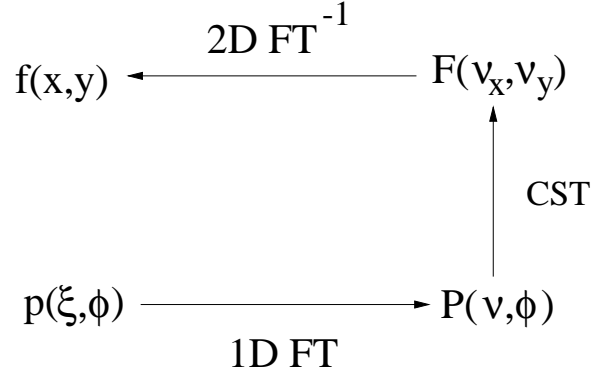
Figure 7. Flow of direct Fourier reconstruction.

- The filtered backprojection algorithm (FBP):

  - Derivation:

$$
\begin{aligned}
f(x,y) &= \int_{-\infty}^{\infty}\int_{-\infty}^{\infty} d\nu_y d\nu_x F(\nu_x,\nu_y)\mathrm{e}^{-j2\pi\nu_x x}\mathrm{e}^{-j2\pi\nu_y y} &(6)\\
&= \int_0^{2\pi} d\phi \int_0^{\infty} d\nu\,\nu\, F(\nu\cos\phi,\nu\sin\phi)\mathrm{e}^{-j2\pi\nu x\cos\phi}\mathrm{e}^{-j2\pi\nu y\sin\phi} &(7)\\
&= \int_0^{2\pi} d\phi \int_0^{\infty} d\nu\,\nu\, P(\nu,\phi)\,\mathrm{e}^{-j2\pi\nu(x\cos\phi+y\sin\phi)} &(8)
\end{aligned}
$$

Using Eq. (5), we have

$$
\begin{aligned}
&\int_\pi^{2\pi} d\phi \int_0^{\infty} d\nu\,\nu\, P(\nu,\phi)\mathrm{e}^{-j2\pi\nu(x\cos\phi+y\sin\phi)}\\
&= \int_0^{\pi} d\phi \int_0^{\infty} d\nu\,\nu\, P(-\nu,\phi)\mathrm{e}^{-j2\pi\nu(x\cos(\phi+\pi)+y\sin(\phi+\pi))}\\
&= \int_0^{\pi} d\phi \int_{-\infty}^{0} d\nu\,(-\nu)\, P(\nu,\phi)\mathrm{e}^{-j2\pi\nu(x\cos\phi+y\sin\phi)}
\end{aligned}
$$

Therefore,

$$
\begin{aligned}
f(x,y) &= \int_0^{\pi} d\phi \int_{-\infty}^{\infty} d\nu\,|\nu|\, P(\nu,\phi)\,\mathrm{e}^{-j2\pi\nu(x\cos\phi+y\sin\phi)} &(9)\\
&= \int_0^{\pi} d\phi\, p'(x\cos\phi + y\sin\phi,\phi) &(10)
\end{aligned}
$$

where

$$
\begin{aligned}
p'(\xi,\phi) &= \int_{-\infty}^{\infty} |\nu|\, P(\nu,\phi)\,\mathrm{e}^{-j2\pi\nu\xi}d\nu &(11)\\
&= p(\xi,\phi) \star b(\xi) &(12)
\end{aligned}
$$

- Hence, $f(x,y)$ can be obtained by backprojection of $p'(\xi,\phi)$ (cf. Eq. (3)).
- The filtered projection profile $p'(\xi,\phi)$ is obtained by applying the *ramp filter* $b(\xi)$, defined in the frequency space as $B(\nu) = |\nu|$, to $p(\xi,\phi)$.
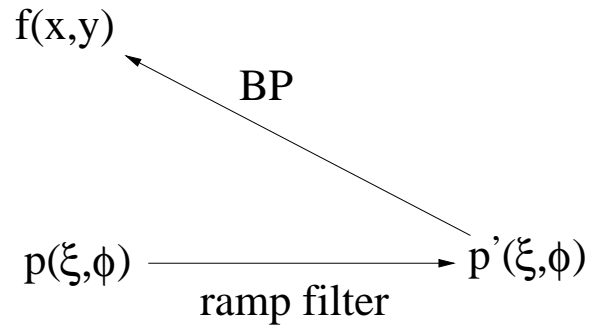- The FBP algorithm is the most widely used algorithm in clinics.

5

f(x,y)

BP

$p(\xi,\phi)$ ⟶ $p'(\xi,\phi)$

ramp filter

Figure 8. Flow of the FBP algorithm.

- Demonstration of the FBP algorithm:

1 view   2 views   10 views

original image

FBP image

30 views   50 views   80 views

backprojection
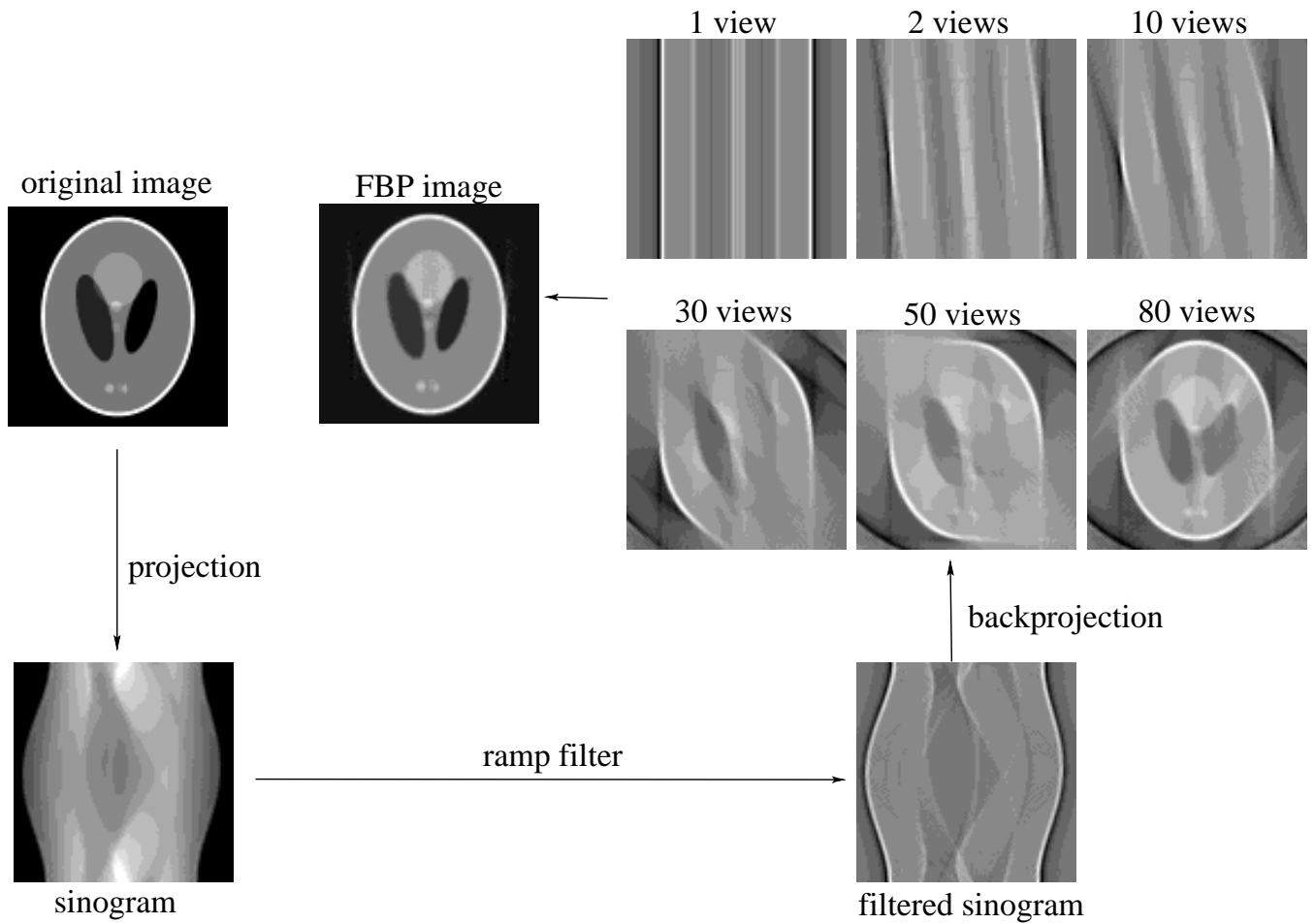
projection

ramp filter

sinogram

filtered sinogram

Figure 8. Demonstration of the FBP algorithm.

6 Practical Issues and Artifacts

- Aliasing - Insufficient angular sampling

  - reducing the number of projections is desirable for the purpose of
    * reducing scanning time
    * reducing noise
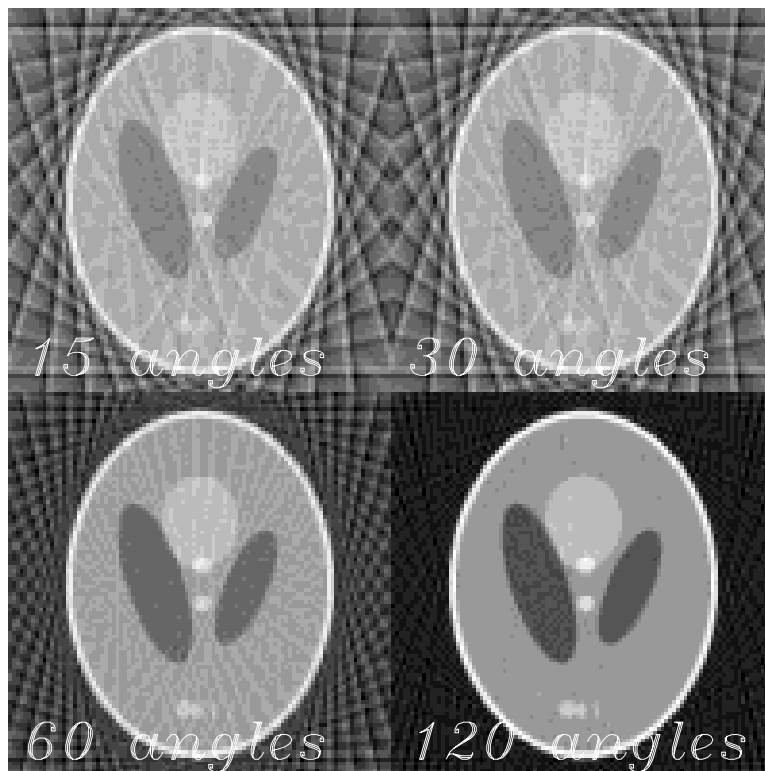   * reducing motion artifact
    * reducing patient dose

Figure 9. FBP images of the Shepp-Logan phantom from various numbers of views.

- Aliasing - Insufficient radial sampling

  - occurs when there is a sharp intensity change caused by, for example, bones.
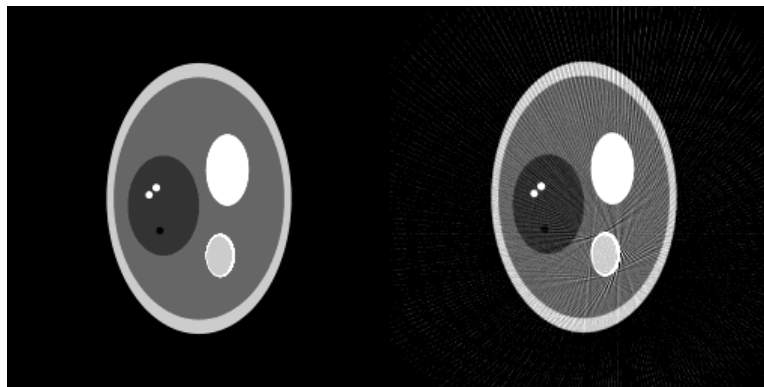

Figure 10. FBP images demonstrating aliasing artifacts.

- Incomplete/Missing data

- portion of data can not be acquired due to physical or instrumental limitations
  * limited angles: Some views can not be acquired due to physical or instrumental limitations (see Fig. 8).
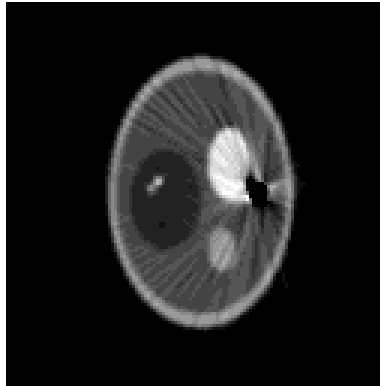 * metal artifacts: In CT, metal blocks the radiation, leading to missing data in its shadow.

Figure 11. metal artifacts.

- Motion artifact

  - caused by patient motion, such as respiration and heart beat, during data acquistion
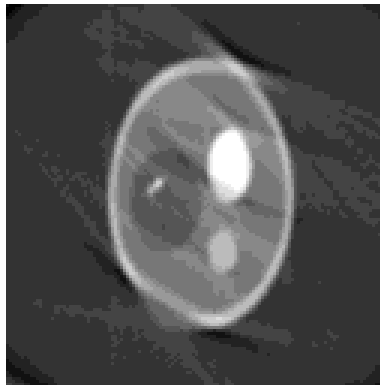

Figure 12. Artifacts caused by patient motion.

- Noise

  - photon detection is a stochastic process
  - lower noise level can be obtained by increasing the radiation dose, and/or the acquisition time.
  - as demonstrated below, perception of structures depends on the contrast, size, and noise level:
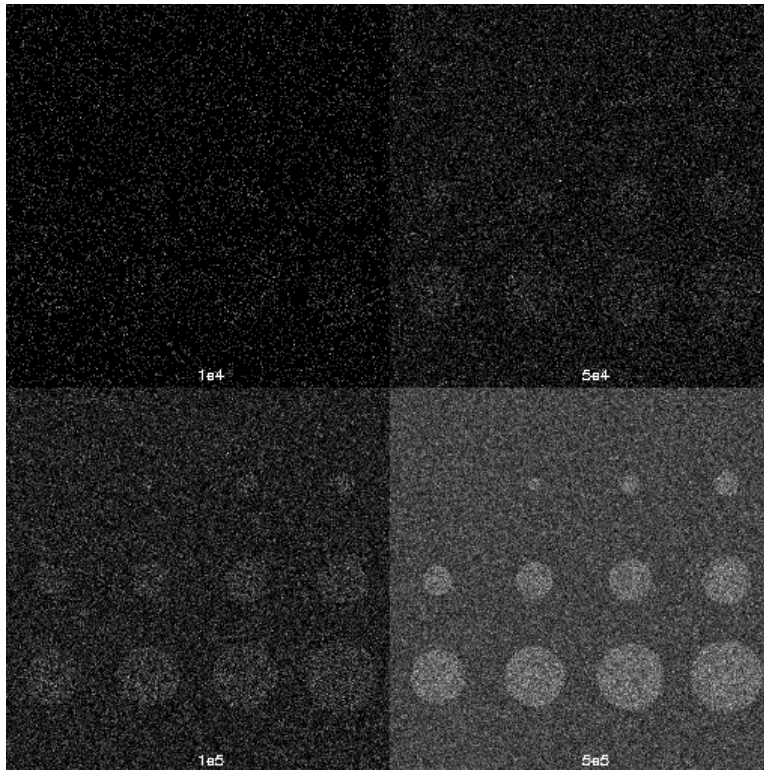
Figure 13. Effect of noise on image quality.

- Finite resolution

    - finite detector size limits the resolution of the acquired data

Figure 14. Effect of finite Resolution on the image quality.
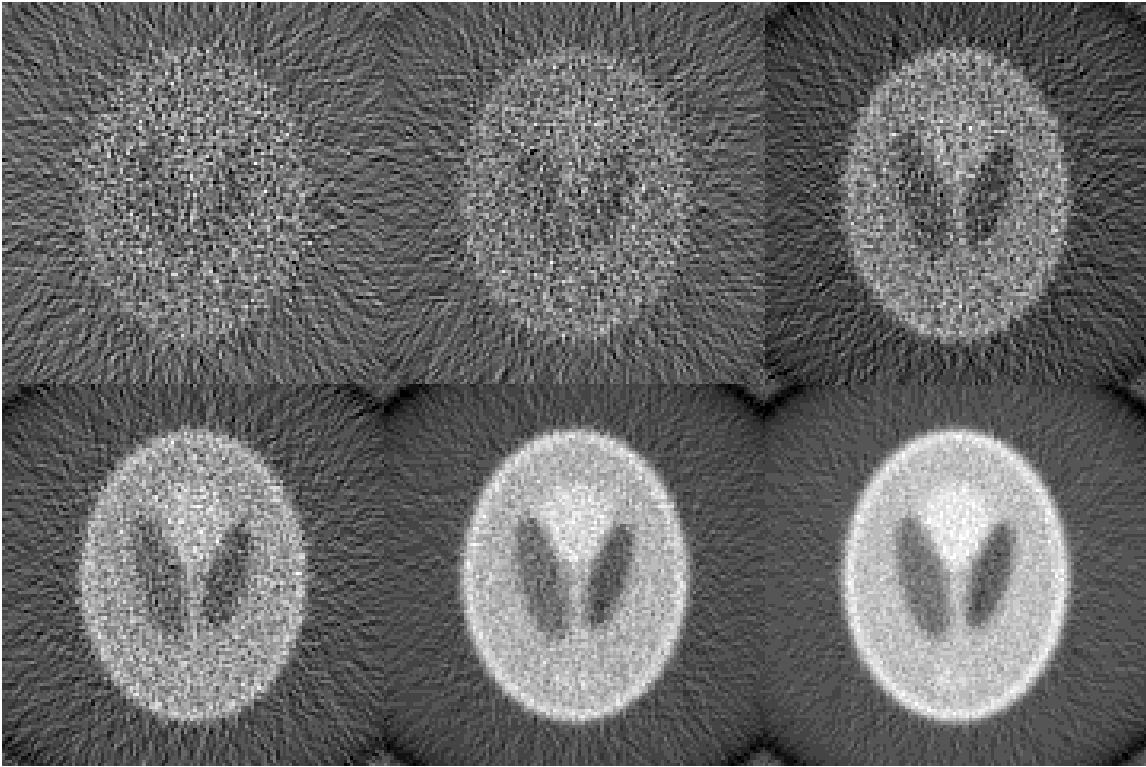
- FBP images of noisy and blurred sinograms:

Figure 15. FBP images of the Shepp-Logan phantom with finite resolution and limited photon counts.

- Others: partial volume effect, beam hardening, ...